Pharm Res (2015) 32:2328–2343
DOI 10.1007/s11095-015-1625-2

RESEARCH PAPER

RGD Peptide-Pegylated PLLA Nanoparticles Containing Epirubicin Hydrochloride Exhibit Receptor-Dependent Tumor Trafficking *In Vitro* and *In Vivo*

Ping Huang • Jun Wu • Ximeng Li • Xiaozheng Liu • Yinghuan Li • Guohui Cui

Received: 6 June 2014 / Accepted: 7 January 2015 / Published online: 16 January 2015

ABSTRACT

Purpose A novel hydrophilic conjugate of arginine-glycine-aspartic acid (RGD) and polyethylene glycol (PEG), i.e., RGD-PEG_{Mw} (M_W = 300, 600, 1000 or 4000), was synthesized and employed in epirubicin (EPI) loaded poly L-lactic acid (PLLA) nanoparticles (NPs) to improve its tumor targeting effect.

Methods *In vitro* studies were performed to assess EPI release from NPs in tumor-mimic acidic medium, cytotoxicity and cell cycle assay in HepG2 cells, and cellular uptake kinetics in four types of tumor cells including A375 cells (high integrin receptor expression), HeLa cells (low integrin receptor expression), and metabolic HepG2/SMMC7721 cells. *In vivo* pharmacodynamics (PD) and pharmacokinetic (PK) studies were determined in a murine ascites tumor model.

Results Cellular uptake kinetics showed integrin receptor-dependent binding and internalization. *In vitro* release results showed that PLLA and PEG groups retarded EPI release from NPs and promoted drug release amount in acidic medium, which benefited *in vivo* trafficking to the acidic tumors. *In vivo* PD and PK studies revealed that RGD-PEG_{Mw} (M_W = 600 ~ 1000) improved tumor targeting capacity of NPs by ~2.4-fold, compared to conventional EPI NPs.

Conclusions RGD-PEG_{Mw} (M_W = 600 ~ 1000) modified PLLA NPs provide a promising strategy to improve tumor selectivity in cancer treatment.

KEY WORDS cellular uptake · nanoparticles · PEG · RGD · tumor targeting

ABBREVIATIONS

B and B_{eq}	Cell membrane-bound EPI fluorescence intensity at time t and at equilibrium
CL	Clearance
EE	Entrapment efficiency
EPI	Epirubicin hydrochloride
FI	Fluorescence intensity
GGD	Glycine-glycine-aspartic acid
GGD-PEG_{600}	Glycine-glycine-aspartic-polyethylene glycol 600
GGD-PEG_{600}-NPs-EPI	Epirubicin nanoparticles containing glycine-glycine-aspartic-polyethylene glycol 600
I and I_{eq}	Intracellular EPI fluorescence intensity at time t and at equilibrium
IRW	Increment ratio of body weight
*M*w	Molecular weight
NPs	Nanoparticles
NPs-EPI	Conventional epirubicin nanoparticles
NPs-PLLA	Blank nanoparticles preparation

Electronic supplementary material The online version of this article (doi:10.1007/s11095-015-1625-2) contains supplementary material, which is available to authorized users.

P. Huang • X. Li • X. Liu • Y. Li (✉) • G. Cui (✉)
School of Chemical Biology and Pharmaceutical Science
Capital Medical University, 10 Xitoutiao, You Anmen
Fengtai District, Beijing 100069, China
e-mail: liyinghuan@ccmu.edu.cn

Y. Li
e-mail: huan694@hotmail.com
e-mail: cgh@ccmu.edu.cn

J. Wu
College of Pharmacy, University of South Carolina
Greenville, South Carolina 29607, USA

PEG_{600}-NPs-EPI	Epirubicin nanoparticles containing polyethylene glycol 600
PEG_{Mw}	Polyethylene glycol (*Mw* = 300, 600, 1000, 4000)
PI	Polydispersity index
PLLA	Poly-L-lactic acid (*Mw* = 12000)
RGD	Arginine-glycine-aspartic acid
RGD-NPs-EPI	Epirubicin nanoparticles containing arginine-glycine-aspartic acid
RGD-PEG_{600}-NPs	Blank nanoparticles preparation containing arginine-glycine-aspartic-polyethylene glycol 600
RGD-PEG_{Mw}	Arginine-glycine-aspartic-polyethylene glycol with different molecular weights (*Mw* = 300, 600, 1000, 4000)
RGD-PEG_{Mw}-NPs-EPI	Epirubicin nanoparticles containing arginine-glycine-aspartic-polyethylene glycol with different molecular weights (*Mw* = 300, 600, 1000, 4000)
RTI	Relative targeting index
TC and TC_{eq}	Total cell-associated EPI fluorescence intensity at time t and at equilibrium
T_{eq}	Time to reach equilibrium or steady state of binding
TGI	Tumor growth inhibition
ZP	Zeta potential

INTRODUCTION

Biomaterials, such as peptide-conjugated synthetic polymers, play an important role in modern drug delivery system as designable biophysical and biochemical ligands to actively target tumors. Arginine-glycine-aspartic acid (RGD) as an integrin-adhesive peptide has been successfully conjugated to various amino acids to form RGDX (e.g., X = C, Q, S, F, V, Y, L, or W) [1–3]. The binding affinity of RGD with integrins by the fourth amino acid X and the use of RGDX-linked carrier as an active targeting delivery system to tumors have been reported by previous studies. For example, conjugate RGDX with bioreducible polymer poly (CBA-DAH) or the use of RGDX-fatty acids/alcohols/amines in liposomal formulations for cancer therapy [1, 3, 4]. The tetrapeptide RGDX conjugates have been shown as potent ligands adhering to integrin receptors on tumor cell surface. The hydrophobicity of the fourth amino acid X was found to enhance the binding affinity of RGDX with integrins, likely via affecting the conformation or directly changing binding capacity. Since RGD is hydrophilic, easily degraded and has a short half-life *in vivo*, the tripeptide RGD alone has been shown as an invalid ligand for integrin-adhesion. Evidence showed that the fourth amino acid X can be successfully replaced by a linking group (fatty alcohol) to connect RGD and liposomes without reducing its binding affinity to integrins [5]. The lipophilic fatty alcohol may promote RGD-fatty alcohol's tumor-targeting capacity. Therefore, the research question of this study is whether a hydrophilic group connecting to RGD has the same effect on enhanced tumor-targeting capacity as the fatty alcohol does.

Polyethylene glycol (PEG) is known as hydrophilicity, neutral charge, non-toxicity and non-immunogenicity with stealth property to avoid protein adsorption and clearance by mononuclear phagocyte system (MPS) [6]. These superiorities make PEG biocompatible for *in vitro* and *in vivo* experiments, and also attractive for synthetic chemistry [7, 8]. On the whole body level, PEG modified nanoparticles (NPs) contribute to long circulation time, which benefits the passive tumor targeting via the enhanced permeability and retention (EPR) effect caused by the leaky vasculature and absence of lymphatic drainage in tumors [9]. On the cellular level, PEG has been shown reduced tumor cellular uptake of NPs due to its stealth effect. Therefore, RGD-PEG conjugate was designed and synthesized to combine RGD bioactivity and PEG stealth property. RGD may conquer the cellular uptake deficiency of PEG and on the contrary PEG may improve the body level trafficking to tumors. We hypothesized that nanoparticles containing RGD-PEG conjugate is an effective ligand to enhance tumor trafficking.

This paper examined the tumor selectivity of RGD-PEG conjugate modified poly-L-lactic acid (PLLA) NPs. PLLA was adopted to prepare NPs owing to its good biocompatibility, biodegradation, pH-sensitivity and relatively low cytotoxic properties [10, 11]. PEG also worked as a linking group between RGD and NPs to prevent RGD dropping from NPs. The effective molecular weight (M_W) of PEG chain in RGD-PEG_{Mw} (M_W = 300, 600, 1000, or 4000) was measured. Glycine-glycine-aspartic acid (GGD) and PEG_{600} conjugate (GGD-PEG_{600}) was also synthesized by changing R to G in RGD-PEG to examine the effects of amino acid sequence on tumor selectivity. Epirubicin Hydrochloride (EPI), an anthracycline drug clinically widely-used for chemotherapy by intercalating DNA strands which finally lead to cell death, was selected as a model drug [12]. The *in vitro* assessment (EPI release, tumor cellular uptake kinetics, cytotoxicity and cell cycle assay) and *in vivo* pharmacodynamics (PD) and pharmacokinetic (PK) studies of EPI NPs containing various RGD-PEG_{Mw} were determined.

MATERIALS AND METHODS

Materials

Epirubicin Hydrochloride (EPI, pharmaceutical grade, Batch No:HF070807) was obtained from HuaFeng United

Technology Co., Ltd. (Beijing, China). Poly-L-lactic acid (PLLA, M_W = 12000) was obtained from Weiqi Boxing Biochemical Technology Co. Ltd. (Wuhan, China). Polyethylene glycol (PEG, M_W = 300, 600, 1000, or 4000) were obtained from Sinopharm Chemical Reagent Co., Ltd. (Beijing, China). All amino acids and their protected forms were L isomers and were obtained from GL Biochem Ltd. (Shanghai, China). Dicyclohexylcarbodiimide (DCC), 1-hydroxybenzotriazole (HOBt) and Pd/C were also from GL Biochem Ltd. Dimethylformamide (DMF), tetrahydrofuran (THF), N-methylmorpholine (NMM), dichloromethane (CH_2Cl_2), methanol, NaOH, ethyl acetate (EA), Tween 80 and all the ingredients needed for phosphate buffered saline (PBS) were purchased from Beijing Chemical Works (Beijing, China). Dimethyl sulfoxide (DMSO) was from Acros Organics, 4',6-diamidino-2-phenylindole (DAPI) from Roche and Guava cell cycle regent from Millipore (USA). 3-(4,5-dimethylthiazol-2-yl)-2,5-diphenyltetrazolum bromide (MTT), penicillin and streptomycin were from Amresco (Ohio, USA). Trypsin (0.25%) was obtained from Sigma-Aldrich (USA). All the reagents and chemicals were of analytical or HPLC grade unless otherwise specified and were used without further purification. DMEM, RPMI-1640 media and fetal bovine serum (FBS) were obtained from Shanghai Bioleaf Biotch Co., Ltd. (HyClone®, Shanghai, China).

Cell Culture

All cell lines were cultivated at 37°C in a 5% CO_2 incubator. Human carcinoma cells, HepG2, SMMC7721, A375 and HeLa were purchased from Beijing Cancer Hospital (Beijing, China). HepG2, A375 and HeLa cells were cultured in DMEM and SMMC7721 cells were cultured in RPMI-1640, supplemented with 10% heat-inactivated FBS, 100 IU/ml penicillin and 100 IU/ml streptomycin.

Animals

Male Kunming mice (25–28 g), supplied by the Animal Services, Capital Medical University (Beijing, China), were maintained at 25°C and 55% of humidity under natural light/dark conditions. Animal experiments complied with the "Principle of Laboratory Animal Care" and were carried out in accordance with the protocol approved by the Experimental Animal Care Committee of Capital Medical University.

Synthesis of RGD-PEG$_{Mw}$

RGD-PEG$_{Mw}$ (M_W = 300, 600, 1000, or 4000) were synthesized respectively as described in Fig. 1A. N-α-tert-butyloxycarbonyl-N-γ-nitro-L-arginine [Boc-Arg (NO_2)-OH] and tosylated glycine benzyl ester (Tos·H-Gly-OBzl) were condensed into Boc-Arg (NO_2)-Gly-OBzl via amido bond, followed by selective removal of the benzyl ester group at the C-terminus to yield Boc-Arg (NO_2)-Gly-OH. Tosylated aspartic dibenzyl ester [Tos·H-Asp-(OBzl)$_2$] was then added in the reaction to yield Boc-Arg (NO_2)-Gly-Asp-(OBzl)$_2$ through amide condensation and further to obtain Boc-Arg (NO_2)-Gly-Asp (OH)$_2$ by selective de-protection, followed by PEG linkage at two-fold excess through carbonyl condensation reaction. The final polymers RGD-PEG$_{Mw}$ were yielded by de-protection of N-tert-butyloxycarbonyl (Boc) and nitro groups and then dialysis (M_W cut off, 3500 Da) for purification and lyophilization [13]. GGD-PEG$_{600}$ was synthesized as a control using the same method by replacing Boc-Arg (NO_2)-OH with Boc-Gly-OH at the beginning of reaction. RGD-PEG$_{300}$, RGD-PEG$_{600}$ and GGD-PEG$_{600}$ were light yellow grease, while RGD-PEG$_{1000}$ was paste and RGD-PEG$_{4000}$ was solid. The final products were stored at −20°C.

Preparation of EPI NPs Containing RGD-PEG$_{Mw}$

EPI NPs containing various RGD-PEG$_{Mw}$ conjugates (M_W = 300, 600, 1000) were prepared by emulsion solvent evaporation method [14]. Briefly, EPI solution (3.3 mg/ml, 3 ml) was added in form of drops into CH_2Cl_2 (25 ml) containing PLLA (60 mg) and RGD-PEG$_{Mw}$ (0.026 mmol, equal to 9 mg RGD) slowly under moderate magnetic stirring to form the original emulsion. After ultrasound at 200 W in ice-water using a water bath sonicator (KQ-500E, Xin zhi Biotechnology Co. Ltd., China) for 3 min, the original emulsion was syringed into Tween 80 aqueous solution (1%*w*/*v*, 37 ml) quickly under moderate magnetic stirring to form multiple emulsions. After CH_2Cl_2 was evaporated, the RGD-PEG$_{Mw}$-NPs-EPI (M_W = 300, 600, or 1000) were obtained. Similarly, RGD-PEG$_{4000}$-NPs-EPI was prepared as a control for *in vivo* PD study to assess the effects of molecular weights of PEG on the tumor targeting capacity of RGD-PEG$_{Mw}$.

Blank NPs (NPs-PLLA), RGD-PEG$_{600}$ modified blank NPs (RGD-PEG$_{600}$-NPs), conventional EPI NPs (NPs-EPI), RGD modified EPI NPs (RGD-NPs-EPI), PEG$_{600}$ modified EPI NPs (PEG$_{600}$-NPs-EPI) and GGD-PEG$_{600}$ modified EPI NPs (GGD-PEG$_{600}$-NPs-EPI) were prepared using the same method as controls for *in vitro* and *in vivo* experiments. The free EPI was removed by size exclusion chromatography on a Sephadex G50 column and then the entrapment efficiency (EE) and drug contents in NPs were determined by Shimadzu UV-visible spectrophotometer at 480 nm [15].

The particle size, polydispersity index (PI) and zeta potential (ZP) were measured by dynamic light scattering (DLS) on a ZetaPALS instrument (Brookhaven Instruments Corp., Worcestershire, NY). The morphology of EPI NPs was observed under transmission electron microscope (TEM, JEM-1230, JEOL, Japan) and scanning electron microscope (SEM, JSM-6360LV, JEOL, Japan). Differential scanning

calorimetry (DSC, Netzsch, Germany) experiments were conducted to determine the interactions among EPI, PLLA and RGD-PEG$_{Mw}$ and to identify crystalline state of EPI presented in NPs.

In Vitro EPI Release from NPs

To mimic blood neutral and tumor acidic microenvironment, dynamic dialysis method was adopted to investigate EPI release from various NPs at pH 7.4 and 5.4 respectively [16]. NPs containing 0.4 mg EPI were put into a dialysis bag (M_W cut off, 3500 Da) and the end-sealed dialysis bag was incubated at 37°C for 72 h in 35 ml of PBS (pH 7.4 or 5.4), with stirring at 140 rpm. Full medium was extracted at predetermined time intervals and replaced with fresh PBS. The amount of EPI released from NPs was determined by UV-visible spectrophotometer at 480 nm.

Cytotoxicity Assay

In vitro cytotoxicity of various EPI NPs was measured by a MTT assay. HepG2 cells were seeded in 96-well plates at 3×10^4 cells per well and incubated at 37°C for 24 h prior to drug addition. The culture medium was replaced with medium containing serial dilutions of various EPI formulations, including RGD-PEG$_{600}$-NPs-EPI, GGD-PEG$_{600}$-NPs-EPI, NPs-EPI and EPI solution. RGD-PEG$_{600}$-NPs-EPI was randomly adopted as an example of RGD-PEG$_{Mw}$-NPs-EPI. Cells were incubated for an additional 24 h, 48 h and 72 h, respectively. Cells were then washed once with PBS and cultured in MTT PBS solution (1 mg/ml, 100 μL/well) for 4 h at 37°C. Medium was then replaced with DMSO (100 μL/well) to dissolve the resulting formazan crystals from MTT. Cell viability was evaluated by absorbance of formazan crystals at 490 nm on a Bioradmicroplate reader (Model 680, Japan).

Cell Cycle Analysis

The cell cycle distribution of EPI NPs treated by HepG2 cells was analyzed. Cells were seeded in 6-well plates at 2×10^5 cells per well for 24 h, followed by the addition of RGD-PEG$_{600}$-NPs-EPI, NPs-EPI and EPI solution (0.6 mg/ml EPI) and incubation at 37°C for 6, 12, 24, 48 and 72 h, respectively. At predetermined time point, cells were collected and fixed in 75% cold ethanol at −20°C for 1 h, followed by centrifugation twice to remove ethanol. Cells were then resuspended in 200 μL Guava cell cycle regents. After another 30 min of incubation at room temperature in darkness, cells were analyzed on a Guava easycyte mini flow cytometer (Millipore, USA). Data analysis was performed using cell-quest software (Becton Dickinson, USA).

Cellular Uptake Kinetics

RGD-PEG$_{600}$-NPs-EPI was selected to further examine the effect of RGD-PEG$_{600}$ on cell membrane binding and subsequent internalization of EPI NPs. Four EPI formulations (RGD-PEG$_{600}$-NPs-EPI, GGD-PEG$_{600}$-NPs-EPI, NPs-EPI and EPI solution) and four types of tumor cells (A375, HeLa, HepG2 and SMMC7721 cells) were selected to examine the time-dependent and concentration-dependent behaviors of cellular uptake kinetics. A375 cells are known as overexpressing $\alpha_v\beta_3$ integrin receptors, while HeLa cells show relatively low integrin expression [17, 18]. Human hepatocellular carcinoma cell lines HepG2 and SMMC7721, as the representative of metabolism cells, were included to measure active targeting potent of RGD-PEG$_{600}$ to various tumor cells.

Confocal Fluorescence Microscopic Analysis of Cell Membrane Binding and Internalization of EPI NPs

A375 cells were seeded on glass bottom micro-well dishes (Mat Tek Corporation) overnight to allow the formation of a monolayer and then incubated with the aforementioned EPI formulations at a final medium concentration of 2 μg/ml EPI at 37 and 4°C for 2 h, respectively. The cells were then washed three times with ice-cold PBS and fixed in 70% ethanol for 20 min. After staining the cell nuclei with DAPI (100 ng/ml in PBS) for 10 min, the cells were covered with glycerol (90%) and then examined under a confocal microscope (LEICA TCS SP5, Germany). The excitation/emission wavelengths were 401/421 and 495/558 nm for DAPI (blue) and EPI (red), respectively.

Quantitative Analysis of Cell Membrane Binding and Internalization of EPI NPs by Flow Cytometry

A375 cells were seeded in 24-well plates and allowed to reach a density of 2.5×10^5 cells/well. The cells were washed once with PBS and then incubated with 1 ml DMEM at 37°C for 30 min. After the medium was replaced with a suspension of EPI NPs, the plates were incubated at 37 and 4°C for 0–6 h. At predetermined time points, culture medium containing EPI NPs disassociated from cells was removed. The attached cells were washed three times with ice-cold PBS and then were detached by trypsin (0.25%, 200 μL/well, Sigma). After washed with ice-cold PBS three times, the cells were

Fig. 1 Synthesis of RGD-PEG$_{Mw}$ (*Mw* = 300, 600, 1000, 4000). **A** The synthesis route was under ice bath: (I) NMM, HOBt and DCC; (II) 2 N NaOH; (III) HOBt and DCC; (IV) 4 N HCl-EA, 5% Pd/C and H_2 (0.02 MBa). The *blue groups* and *red groups* in the chemistry structural formula are available reaction groups and newly-formed groups in each step, respectively. **B** The peak assignments for RGD-PEG$_{Mw}$ (Take *Mw* = 1000 as an example) in the spectra of FTIR, ^{1}HNMR and ^{13}CNMR, respectively.

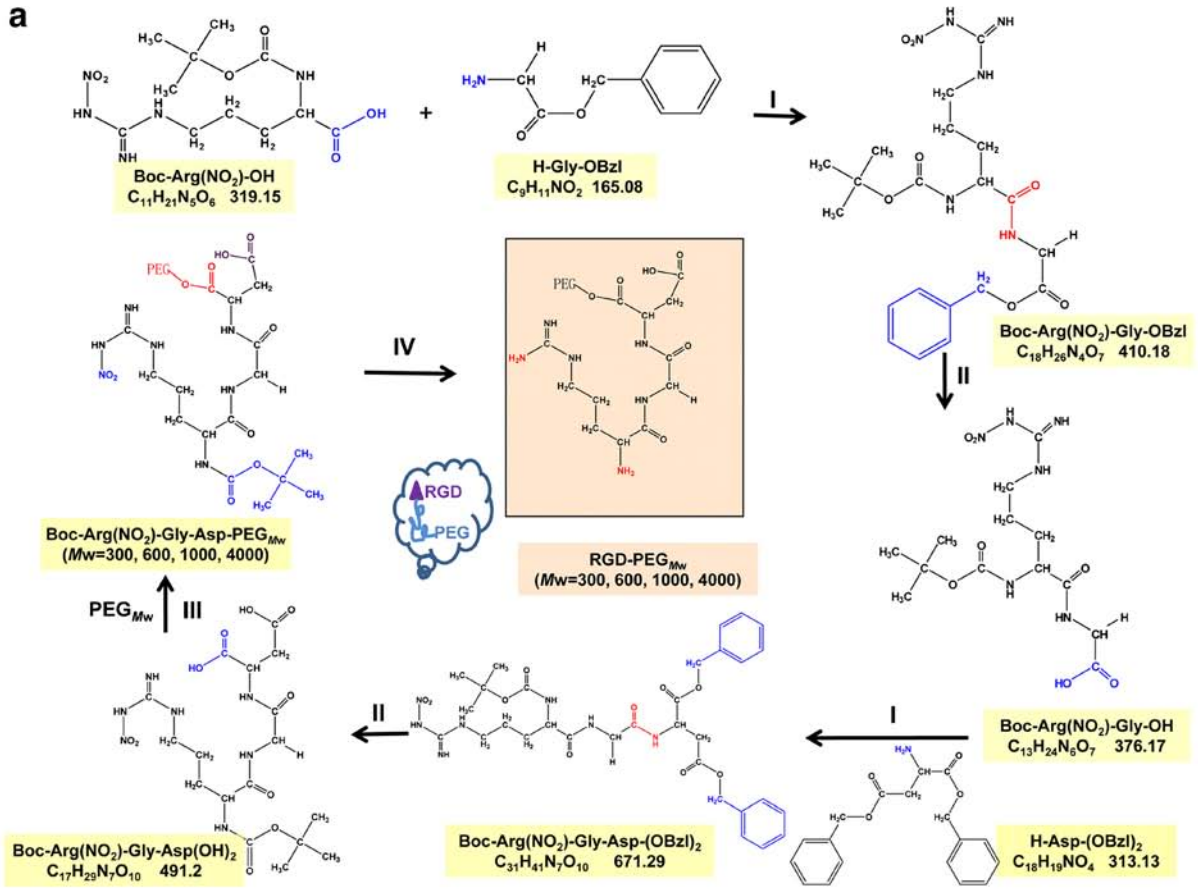
a
Boc-Arg(NO2)-OH
C11H21N5O6 319.15
H-Gly-OBzl
C9H11NO2 165.08
I
Boc-Arg(NO2)-Gly-OBzl
C18H26N4O7 410.18
II
Boc-Arg(NO2)-Gly-OH
C13H24N6O7 376.17
I
H-Asp-(OBzl)2
C18H19NO4 313.13
Boc-Arg(NO2)-Gly-Asp-(OBzl)2
C31H41N7O10 671.29
II
Boc-Arg(NO2)-Gly-Asp(OH)2
C17H29N7O10 491.2
PEGMw
III
Boc-Arg(NO2)-Gly-Asp-PEGMw
(Mw=300, 600, 1000, 4000)
IV
RGD
PEG
RGD-PEGMw
(Mw=300, 600, 1000, 4000)

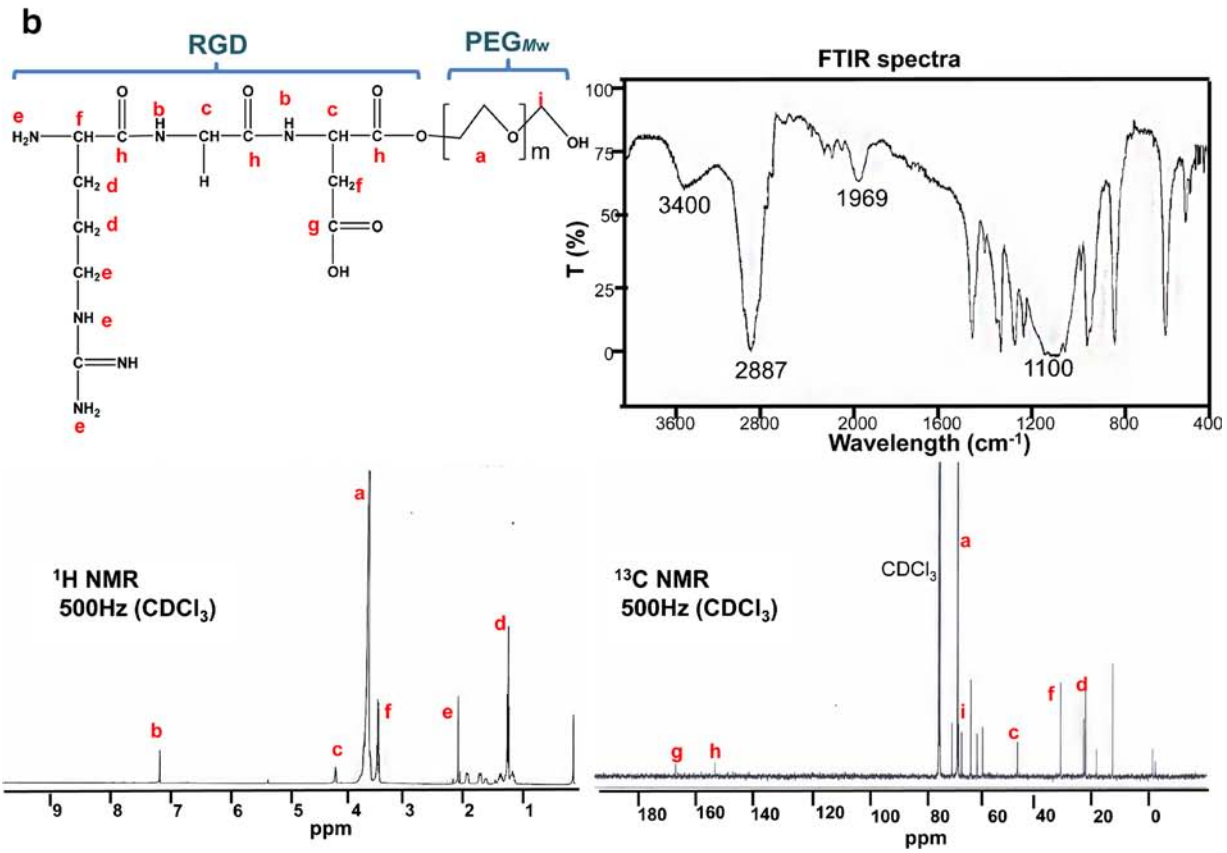
b
RGD
PEGMw
FTIR spectra
T (%)
3400
2887
1969
1100
Wavelength (cm-1)
1H NMR
500Hz (CDCl3)
ppm
13C NMR
500Hz (CDCl3)
CDCl3
ppm

resuspended in 0.5 ml of cold PBS to test the fluorescence intensity of 5000 cells on a Guava easycyte mini flow cytometry. The time-dependent accumulation of EPI from various NPs in A375 cells were measured for 0–6 h at 2 μg/ml of initial extracellular EPI concentration to determine the time to reach the steady state of binding (T_{eq}). The concentration-dependent accumulation of EPI in A375 cells were measured at T_{eq} from 0.5 to 20 μg/ml of initial extracellular EPI concentration and compared to HeLa, HepG2 and SMMC7721 cells respectively to further assess tumor cells selectivity of RGD-PEG_{600} motif.

In Vivo Pharmacodynamics Study

The anti-tumor activity was determined in Kunming mice inoculated with S_{180} sarcoma. Mice were maintained in accordance with institutional guidelines. S_{180} tumor cells passaged in mice abdomen (Vital River Laboratory Animal Technology Co. Ltd., Beijing, China) were harvested on the 8th day after tumor implantation and resuspended in saline at 2.0×10^7/ml, which was injected subcutaneously under the right armpit of each mouse (0.2 ml per mouse). The mice inoculated with S_{180} tumor cells were randomly divided into 13 groups with 10 in each group. After 24 h incubation (day 1), various EPI formulations (40 μg per mouse) were injected intravenously (i.v.) via the tail vein and the injections were repeated on day 4 and day 7. Two days after the final injection, the mice were weighed before sacrifice and tumors were also weighed. Blank NPs including NPs-PLLA, RGD-PEG_{600}-NPs and saline were used as negative controls. EPI solution, NPs-EPI, GGD-PEG_{600}-NPs-EPI and RGD-NPs-EPI were used as positive controls to differentiate the targeting effects of functional groups RGD-PEG_{Mw} in EPI NPs. The effect of molecular weights of PEG on the tumor targeting capacity of RGD-PEG_{Mw} was evaluated by RGD-PEG_{Mw}-NPs-EPI (M_W=300, 600, 1000, or 4000). The body weight and tumor weight of groups given with RGD-PEG_{600}-NPs-EPI at different EPI doses (1, 2, 3 mg/kg) were also investigated. Body weight was calculated as (mouse weight before sacrifice - tumor weight). Increment ratio of body weight (IRW) was calculated as {[(body weight/normal mouse weight before inoculation with S_{180} tumor cells) -1]×100%}. Tumor growth inhibition (TGI) was calculated as [(1-tumor weight of treated group/tumor weight of saline group)×100%]. The higher values of IRW and TGI indicate the better antitumor capability of the formulation.

In Vivo Pharmacokinetic and Biodistribution Study

A total of 144 male Kunming mice inoculated with S_{180} tumor cells under the right armpit were randomly assigned to 3 groups with 48 in each group for pharmacokinetic experiments. After seven-day inoculation, mice received i.v. tail vein injections of EPI solution, NPs-EPI and RGD-PEG_{600}-NPs-EPI, respectively at an equivalent dose of 8 mg/kg EPI *vs.* the body weight (X_0) [19]. Blood samples were collected (n=6) at various time intervals (0.083, 0.25, 0.5, 1, 4, 8, 24, 48 h) and mice were then sacrificed. Tumors, livers, brains and hearts were collected, washed, weighed and stored at −20°C. Liquid-liquid extraction was performed prior to analysis [20]. Briefly, blood or homogenized tissue (1 g of tissue: 3 ml of PBS) were mixed with chloroform and methanol (4:1, *v*/*v*) (3 ml for tumor, brain and liver; 1.5 ml for heart) containing 50 μL of daunorubicin (1 μg/ml) as an internal standard. Samples were extracted on a vortex-mixer (IKA.MSI Minishaker) for 3 min and centrifuged at 1000×g for 10 min. An aliquot of the organic layer was collected, dried and re-dissolved in 180 μL of methanol before HPLC analysis. The concentration of EPI was determined by reverse phase HPLC (Waters 2695) with UV detection at 233 nm, a flow rate of 1 ml/min on a Symmetry C_{18} column (4.6 mm×150 mm, 5 μm particle size), and an isocratic program in a methanol : 0.17% phosphonic acid (45:55, *v*/*v*) solvent system.

The fitting of concentration-time (c-t) curves were performed by a nonlinear least square (NLS) model program developed by Zhu [21]. For EPI c-t curves in the blood after i.v. injections, one-compartment model ($c=c_0\times e^{-kt}$) and two-compartment model ($c=Ae^{-\alpha t}+Be^{-\beta t}$) were compared in the NLS model. For the amount of EPI in tissues, formula zero and formula first were selected in the model as follows [5, 21]:

$$\text{Formula zero}: c=A\left(1-e^{-k_1 t}\right)\ldots t\le T;\quad c=A\left(1-e^{-k_1 T}\right)\times e^{-k_2(t-T)}\ldots t>T$$

$$\text{Formula first}: c=A\left(e^{-k_1 t}-e^{-k_2 t}\right)$$

where A is a coefficient. Formula zero uses parameter T to describe the duration of zero-order absorption when the formulation slowly entered the tissue and followed by first-order elimination. k_1 is the absorption rate constant in the ascending part, and k_2 is the elimination rate constant in the declining region after T of the c-t curve. Formula first has a similar format as the first-order absorption equation in one-compartment model. k_1 is the elimination rate constant, and k_2 is the absorption rate constant. The area-under-concentration-time curve (AUC) was calculated using the trapezoidal rule. The clearance (CL) in blood was calculated as (X_0/AUC).

To evaluate the tumor targeting capacity between formulations, relative targeting index (RTI) was introduced and defined as $[(AUC_{0\sim\infty})^{tumor}_{TDDS}/(AUC_{0\sim\infty})^{liver}_{TDDS}]/[(AUC_{0\sim\infty})^{tumor}_{CDDS}/(AUC_{0\sim\infty})^{liver}_{CDDS}]$. Here, *TDDS* indicates the targeted drug delivery system and *CDDS* indicates the contrast drug delivery system.

Statistical Analysis

Data were expressed as means ± standard deviation (X ± SD). Statistically significant differences among multiple groups were determined using the Tukey test after ANOVA.

RESULTS

Synthesis and Characteristics of RGD-PEG$_{Mw}$

Figure 1B shows the peak assignments of the sample product RGD-PEG$_{Mw}$ (Mw = 1000) in the spectra of ^{1}H and ^{13}C nuclear magnetic resonance (NMR, Avance II 500, Broker, Switzerland) and Fourier transform infrared spectroscopy (FTIR, Prestige-21, SHMADZU). The strong signal of PEG shields that of RGD, due to huge molecular weight and highly repeated structure of PEG [22, 23]. The strong signals of repeated methylene ($-CH_2-$) in PEG backbone $(-CH_2-CH_2-O-)_m$ were at 3.6 ppm in ^{1}HNMR spectrum, at 70 ppm in ^{13}CNMR spectrum, and at 1100 and 2887 cm^{-1} in FTIR. The relatively weak signals of peptide bonds (−CO-NH-) in RGD-motif were shown at 7.2 ppm in ^{1}HNMR spectrum and at 157 ppm in ^{13}CNMR spectrum. The broad vibration absorption around 3400 cm^{-1} in FTIR were attributed to the -OH of the carboxylic acid group (−COOH) and PEG. In addition, the peak at 1969 cm^{-1} was associated with the carbonyl group (−CO-) in RGD-motif. Detailed data for the newly synthesized conjugates in ^{1}HNMR, ^{13}CNMR and FTIR spectrum are shown in the Supplementary Material.

Characterization of EPI NPs

The representative morphology of RGD-PEG$_{600}$-NP-EPI in SEM and TEM is shown in Fig. 2. The spherical cauliflower-like surfaces of EPI NPs were very rough in SEM, which might improve the EPI release from NPs. The "RGD-PEG$_{600}$ corona" on the NPs surface are clearly shown in TEM [22]. All NPs demonstrated a narrow size distribution with mean particle sizes at 190–250 nm, PI around 0.2, and ZP at −20 ~ −30 mV (Table I). The EE of EPI in NPs was around 50% and the drug content within NPs was 8–9% (Table I). The free EPI was kept in NPs in the following experiments except DSC test.

DSC thermograms were performed to determine whether EPI was incorporated into the NPs in its crystalline or amorphous form and to elucidate the interaction of EPI and other ingredients (Fig. 3). The endothermic peaks of EPI (182°C, ΔH = −6.4 J/g, f) were completely absent from various lyophilized EPI NPs (b, d and g) but were observed in two groups of physical mixtures (c and e). In addition, the exothermic peak of crystallized RGD-PEG$_{600}$ (129 ~ 139°C, ΔH = 77 J/g, a; 131 ~ 156°C, ΔH = 55 J/g, b) or PEG$_{600}$ (100 ~ 149°C, ΔH = 37 J/g, d) was kept in the lyophilized NPs.

In Vitro EPI Release from NPs

Controlled and sustained drug release is a desirable property for EPI NPs. The drug release from NPs was performed at 37°C under a simulated physiological condition (pH 7.4) and in an acidic environment (pH 5.4) to assess the feasibility of using PLLA/RGD-PEG$_{Mw}$ (M_W = 300, 600, 1000) as an anti-tumor drug delivery carrier. All tested NPs exhibited sustained EPI release profiles compared to EPI solution and the release of RGD-PEG$_{Mw}$-NPs-EPI was slower than that of NPs-EPI at various pH values as shown in Fig. 4 ($p < 0.01$, **c** *vs.* **e**, **f**, and **h** at pH 7.4; **d** *vs.* **g** at pH 5.4). The differences in drug release profiles suggested that the degradation of PLLA retarded drug release and PEG$_{Mw}$ group formed hydration membranes around NPs to further slow down the dissolution. Furthermore, EPI release from conventional or RGD-PEG$_{600}$ modified NPs increased by 12 or 18% at pH 5.4 compared to that at pH 7.4 ($p < 0.01$, **c** *vs.* **d**; **f** *vs.* **g**, Fig. 4). However, the EPI solution release was similar at pH 5.4 and pH 7.4 media ($p > 0.05$, **a** *vs.* **b**, Fig. 4). These results suggested

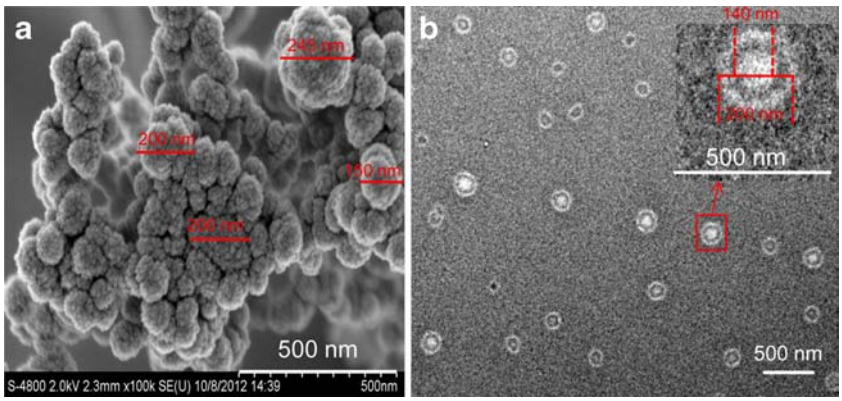

Fig. 2 The morphology of RGD-PEG$_{600}$-NPs-EPI under SEM (**a**) and TEM (**b**). Scale bar 0.5 μm.

Table I Properties of RGD-PEG_{Mw} Linked EPI NPs and Various EPI-Loaded NPs ($n=3$)

Preparation	Size (nm)	PI	ZP (mV)	EE (%)	Actual load (mg EPI/mg NPs)
RGD-PEG_{300}-NPs-EPI	230.9 ± 2.8	0.139 ± 0.004	−27.19 ± 0.66	50.82 ± 3.87	1/11.81
RGD-PEG_{600}-NPs-EPI	231.4 ± 2.0	0.200 ± 0.003	−25.62 ± 0.68	53.89 ± 3.64	1/11.14
RGD-PEG_{1000}-NPs-EPI	219.7 ± 1.2	0.177 ± 0.004	−24.80 ± 0.40	53.14 ± 4.85	1/11.29
GGD-PEG_{600}-NPs-EPI	198.6 ± 2.5	0.186 ± 0.005	−20.00 ± 0.59	50.96 ± 1.05	1/11.78
NPs-EPI	245.5 ± 2.5	0.204 ± 0.008	−24.12 ± 0.58	46.21 ± 3.79	1/12.99
RGD-NPs-EPI	239.7 ± 2.2	0.184 ± 0.008	−26.42 ± 0.85	47.67 ± 3.29	1/12.58
PEG_{600}-NPs-EPI	200.6 ± 1.5	0.199 ± 0.008	−20.77 ± 0.49	52.48 ± 2.15	1/11.43

that the pH-sensitive PLLA played an important role in controlling drug release and RGD-PEG_{600} further delayed the drug release from NPs.

Cytotoxicity Assay

The *in vitro* cytotoxicity of various EPI formulations was measured by IC_{50}, the drug concentration at which 50% of cells have been killed. Table II shows the IC_{50} values of various EPI formulations at 24, 48 and 72 h against HepG2 cells. EPI solution showed the inherent cytotoxicity of EPI. Pegylated EPI NPs reduced the binding of NPs to the cells due to hydration membranes surrounding NPs and showed higher IC_{50} than conventional NPs-EPI. Compared to NPs-EPI, the IC_{50} of RGD-PEG_{600}-NPs-EPI was 1.2 times higher at 24 h, equivalent at 48 h, and 0.8 times lower at 72 h.

Cell Cycle Test

Incubation of HepG2 cells culture medium containing various EPI formulations demonstrated growth arrest. Representative histograms (Fig. 5A) showed the response of HepG2 cells at 24 h as typical EPI distribution at four phases, *i.e.*, sub G1, G0/G1, S and G2/M phase. EPI was well known as cell cycle nonspecific agent blocking DNA replication at S phase and thereby affecting the following phases in the cell cycle such as the synthesis of RNA and proteins to induce apoptosis. Obviously cell growth at G0/G1 phase was suppressed when treated with EPI formulations. Apoptotic cellular fragments appeared at sub G1 phase. Figure 5B depicted the percentages of cells distributed at four phases for various EPI formulations during 0–72 h. The cell distribution at sub G1 phase demonstrated the therapeutic effect of EPI solution reached apex at about 24 h and was gradually attenuated after 24 h. However, the therapeutic effects of NPs-EPI and RGD-PEG_{600}-NPs-EPI kept rising during the period. It may be explained by the increasing slope of sub G1 cell percentage values during 24–72 h, *i.e.*, 0.18, 0.33 and 0.62 for EPI solution, NPs-EPI and RGD-PEG_{600}-NPs-EPI, respectively. The apoptotic cell percentage of RGD-PEG_{600}-NPs-EPI at 72 h of sub G1 phase was nearly 2-fold higher than EPI solution and NPs-EPI. On the contrary, the live cell distribution of RGD-PEG_{600}-NPs-EPI at G0/G1 phase significantly decreased to 5% at 72 h. These results suggested the strong apoptosis induced by RGD-PEG_{600}-NPs-EPI with a prolonged duration.

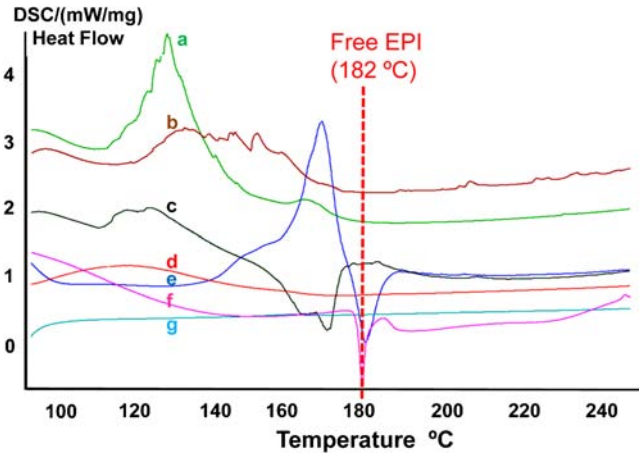

Fig. 3 DSC thermograms of RGD-PEG_{600} (**a**), RGD-PEG_{600}-NPs-EPI (**b**), the physical mixture of RGD-PEG_{600} and free EPI (**c**), PEG_{600}-NPs-EPI (**d**), the physical mixture of PLLA and free EPI (**e**), free EPI solution (**f**) and NPs-EPI (**g**).

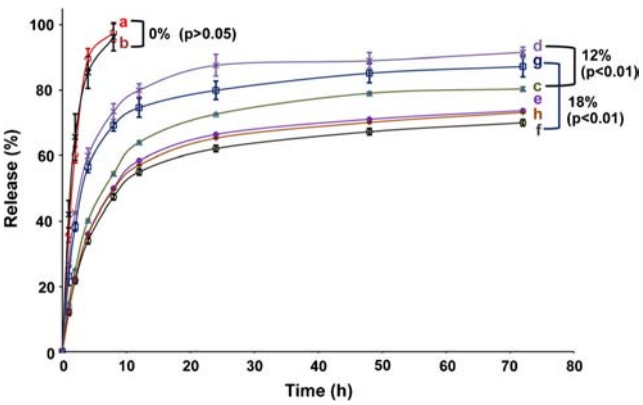

Fig. 4 *In vitro* EPI release profiles from EPI solution (pH = 7.4, **a**; pH = 5.4, **b**), NPs-EPI (pH = 7.4, **c**; pH = 5.4, **d**), RGD-PEG_{300}-NPs-EPI (pH = 7.4, **e**), RGD-PEG_{600}-NPs-EPI (pH = 7.4, **f**; pH = 5.4, **g**), RGD-PEG_{1000}-NPs-EPI (pH = 7.4, **h**) ($n=5$).

Table II Cytotoxicity of Various EPI Formulations to HepG2 Cells ($n = 3$)

EPI formulations	IC_{50} (μM)		
	24 h	48 h	72 h
EPI solution	2.739 ± 0.074	1.125 ± 0.019	0.538 ± 0.009
NPs-EPI	1.622 ± 0.014	0.819 ± 0.017	0.3673 ± 0.053
GGD-PEG_{600}-NPs-EPI	2.159 ± 0.073	0.996 ± 0.010	0.517 ± 0.041
RGD-PEG_{600}-NPs-EPI	$1.846 \pm 0.069^{*\#+}$	$0.815 \pm 0.012^{*+}$	$0.295 \pm 0.038^{*\#+}$

$^{*\#}$ Significant difference ($p < 0.05$) *vs.* EPI (*); NPs-EPI (#); GGD-PEG_{600}-NPs-EPI (+)

Cellular Uptake Kinetics

Qualitative Analysis of Cell Membrane Binding and Intracellular Bioavailability of EPI NPs: Confocal Fluorescence Microscopic Results

Figure 6 shows the confocal microscopy images of A375 cells treated with various EPI formulations for 2 h at 37°C and 4°C. RGD-PEG_{600}-NPs-EPI showed greatest EPI distribution (red) in nuclei at 37°C compared to other EPI formulations. Besides energy-driven cellular uptake, the active targeting groups RGD-PEG_{600} rendered more NPs adhered to cell-surface integrin receptors which facilitated the active internalization [24]. Furthermore, GGD-PEG_{600}-NPs-EPI showed much weaker red fluorescence intensity than NPs-EPI. It may be due to the stealth effect of polymeric NPs induced by hydrophilic PEG coating which reduced the affinity of NPs and cells. However, confocal microscope eliminates out-of-focus signal and only light produced by fluorescence very close to the focal plane can be detected, *i.e.*, the confocal microscopy images are optical cross sectional specimens. Therefore, the binding fluorescence in the stereo cell sphere's surface could not be shown completely.

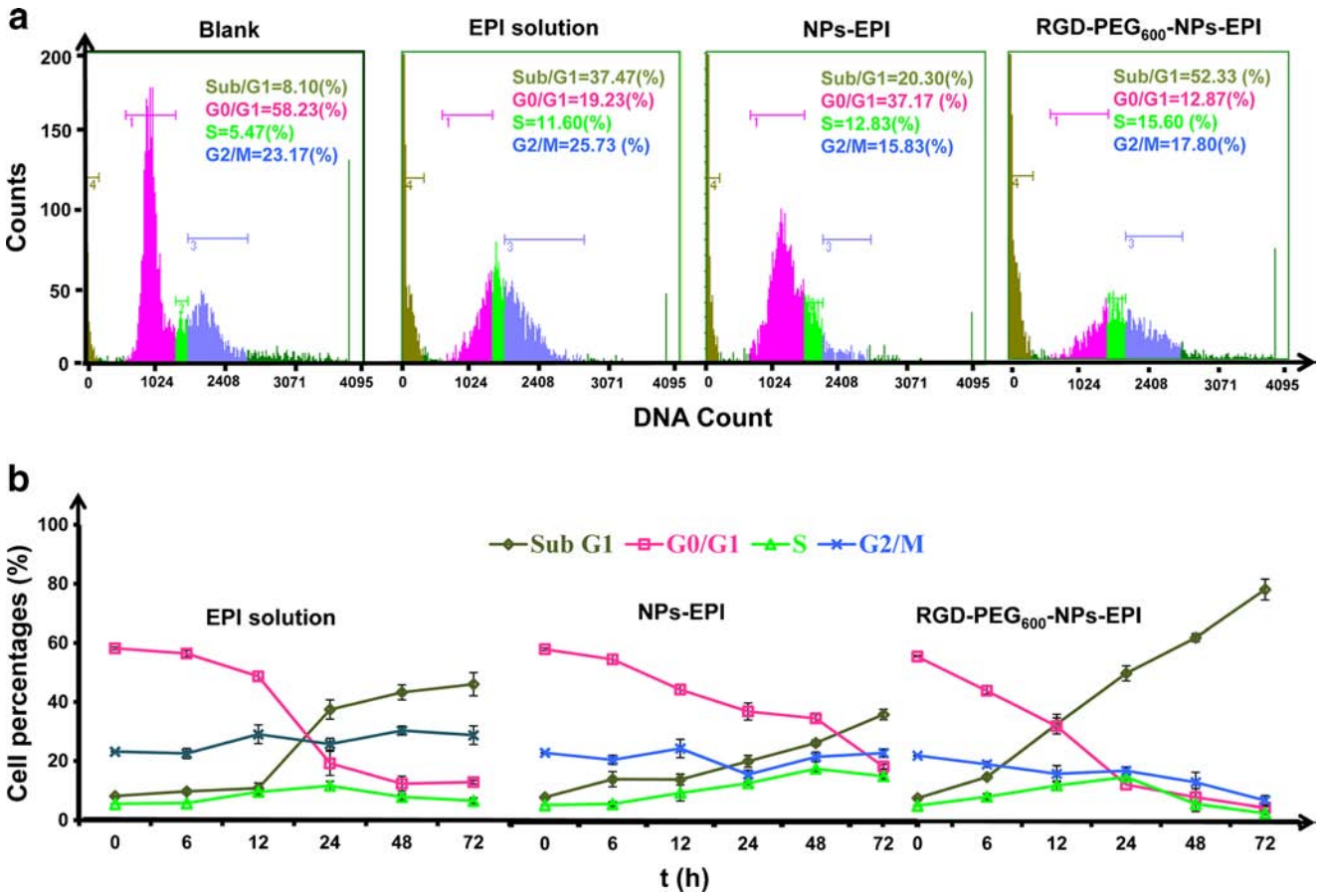

Fig. 5 HepG2 cell cycle distribution after treated with various EPI formulations. **A** Representative histograms of the DNA content at 24 h for untreated cells (Blank) and cells treated with EPI solution, NPs-EPI and RGD-PEG_{600}-NPs-EPI, respectively. **B** The line charts of cell distributed at four phases, i.e., sub G1, G0/G1, S and G2/M phase, for different EPI formulations during 0–72 h.

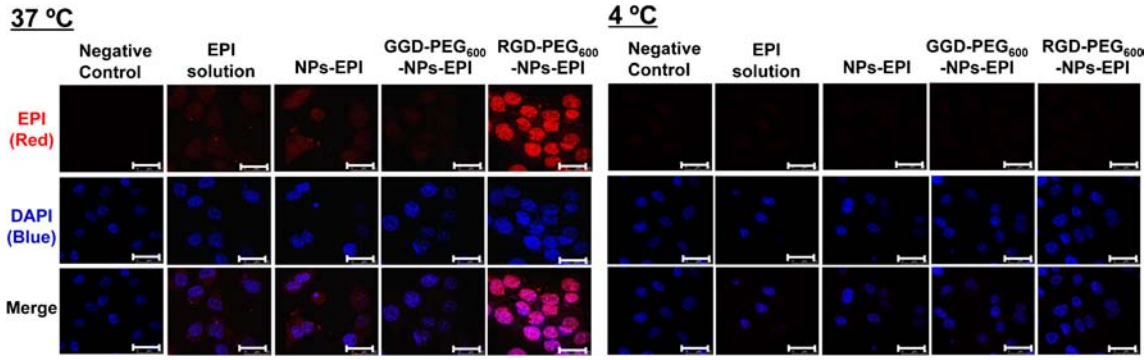

Fig. 6 Confocal microscopy images of A375 cells treated with various EPI formulations, including negative control (no drug treatment),EPI solution, NPs-EPI, GGD-PEG_{600}-NPs-EPI and RGD-PEG_{600}-NPs-EPI, for 2 h at 37 and 4°C, respectively. EPI appears in *red fluorescence*, nucleus appears in *blue fluorescence* (1575× mag). Scale bar 25 μm.

Quantitative Kinetics of Uptake, Cell Membrane Binding, and Internalization of EPI NPs: Flow Cytometry

Flow cytometry collected the whole cell spheres and measured the total fluorescence intensity (FI) including cell-surface binding and internalization. Active targeting superiority of RGD-PEG_{600}-NPs-EPI can be quantitatively calculated by the red FI (i.e., the quantity of EPI) in A375 cells at 37 and at 4°C. The value of $10^{1.5}$ was selected as the threshold of FI value to deduct the background of untreated cells (*i.e.*, the red FI between $10^{1.5}$ and 10^4 was collected, black bar, Fig. 7A). RGD-PEG_{600}-NPs-EPI had the greatest red FI in cells, followed by NPs-EPI, GGD-PEG_{600}-NPs-EPI and EPI solution in turn.

The red FI in cells at 37°C, i.e., the total cell-associated EPI amount (*TC*), may be further separated into cell membrane-bound EPI (*B*) and internalized amount (*I*) based on the published methods [25]. The red FI in cells at 4°C is *B*, and *I* can be calculated as the difference between *TC* and *B*. This temperature-dependent binding/internalization was consistent with the aforementioned confocal fluorescence microscopic results. *I* is the net of intracellular EPI kinetic processes, including internalization of membrane-bound NPs and subsequent process such as endosome-cytosol-nuclei transport, lysosomal degradation, and efflux or recycling. Figure 7B shows the time-dependent accumulation of cell-associated EPI for RGD-PEG_{600}-NPs-EPI, NPs-EPI, GGD-PEG_{600}-NPs-EPI and EPI solution at 2 μg/ml of initial extracellular EPI concentration. In all EPI formulations, the red FI increased with time and reached the steady state at about 4 h. Compared to the other formulations, greater absolute amounts of *TC*, *B* and *I* have been shown in RGD-PEG_{600}-NPs-EPI. Analysis of *I* to *B* ratio (*I*/*B*) over time showed the similar value of *I*/*B* among three NPs, *i.e.*, RGD-PEG_{600}-NPs-EPI, NPs-EPI, GGD-PEG_{600}-NPs-EPI, at the time of steady state (T_{eq}=4 h). The internalization of EPI solution with the lowest *TC*, *B* and *I* was non-endocytosis.

Figure 7B also compares the AUC values of *TC*, *B* and *I*. Compared to EPI solution, NPs-EPI increased the AUCs of *TC*, *B* and *I* by 140, 216 and 102% respectively, demonstrating the predominant superiority of PLLA NPs. Compared to NPs-EPI, GGD-PEG_{600}-NPs-EPI decreased the AUCs of *TC*, *B* and *I* by 22, 11 and 30% respectively and RGD-PEG_{600}-NPs-EPI increased those of *TC*, *B* and *I* by 35, 55 and 19%, respectively. These results suggested that the increased cell uptake associated with RGD could be offset by the PEG groups that may shield RGD with relatively small molecular weight. Compared to GGD-PEG_{600}-NPs-EPI, RGD-PEG_{600}-NPs-EPI increased the AUCs of *TC*, *B* and *I* by 73, 75 and 71%, respectively. The results suggested that RGD greatly improved the binding affinity of NPs with integrins on A375 cell membrane and subsequent internalization.

Figure 7C shows the concentration-dependent accumulation of A375 cell-associated EPI in various formulations at steady state (4 h). TC_{eq}, B_{eq} and I_{eq} representing *TC*, *B* and *I* at 4 h, generally increased with extracellular EPI concentrations and the greatest increase was observed in RGD-PEG_{600}-NPs-EPI, followed by NPs-EPI, GGD-PEG_{600}-NPs-EPI and EPI solution in turn. The relationship

Fig. 7 Cellular uptake kinetics of RGD-PEG_{600}-NPs-EPI (**a**), NPs-EPI (**b**), GGD-PEG_{600}-NPs-EPI (**c**) and EPI solution (**d**). Mean ± SD, n = 3. Some SD are smaller than *symbols*. **A** Flow cytometry analysis of cell-associated EPI red fluorescence intensity (FI). A375 cells were incubated with various EPI formulations at 2 μg/mL of initial extracellular EPI concentration at 37°C for 4 h. The percentage numbers were calculated by the ratio of positive cells number below the line (i.e., cells number corresponding to the red FI between $10^{1.5}$ and 10^4) to the tested cells number (i.e., 5000). **B** Time-dependent accumulation of different EPI formulations in A375 cells at 2 μg/mL of initial extracellular EPI concentration. *TC* cell-associated total EPI FI, *B* cell membrane-bound EPI FI, *I* internalized EPI FI. I/B ratios and AUC were calculated. **C** Concentration-dependent accumulation of different EPI formulations in A375 cells at steady state. Data were obtained after incubation for 4 h or T_{eq}. TC_{eq} cell-associated total EPI FI at T_{eq}, B_{eq} cell membrane-bound EPI FI at T_{eq}, I_{eq} internalized EPI FI at T_{eq}. **D** Concentration-dependent accumulation of RGD-PEG_{600}-NPs-EPI (**a**) and GGD-PEG_{600}-NPs-EPI (**c**) at steady state in HeLa, HepG2 and SMMC7721 cells, respectively.

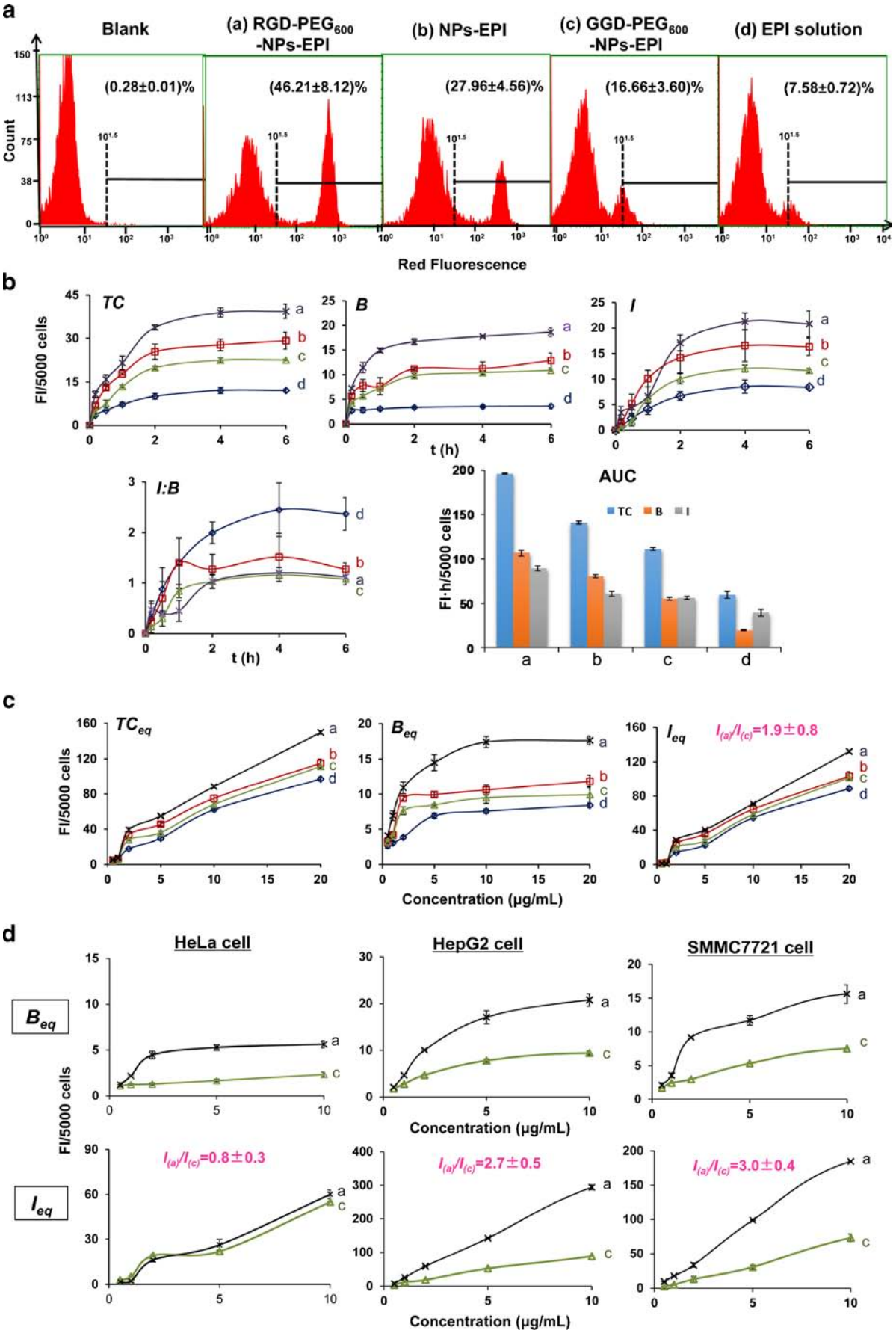
a
Blank
(a) RGD-PEG600 -NPs-EPI
(b) NPs-EPI
(c) GGD-PEG600 -NPs-EPI
(d) EPI solution
(0.28±0.01)%
(46.21±8.12)%
(27.96±4.56)%
(16.66±3.60)%
(7.58±0.72)%
Count
Red Fluorescence
b
TC
B
I
I:B
AUC
Fl/5000 cells
t (h)
Fl·h/5000 cells
TC
B
I
c
TCeq
Beq
Ieq
Fl/5000 cells
Concentration (μg/mL)
I(a)/I(c)=1.9±0.8
d
HeLa cell
HepG2 cell
SMMC7721 cell
Beq
Ieq
Fl/5000 cells
Concentration (μg/mL)
I(a)/I(c)=0.8±0.3
I(a)/I(c)=2.7±0.5
I(a)/I(c)=3.0±0.4

of B_{eq} and initial extracellular EPI concentration appeared to be saturable membrane binding. We observed substantial cell distortion at 20 μg/ml extracellular EPI concentration, which might compromise the data quality. Therefore, 0–10 μg/ml extracellular EPI concentration were selected to further study the concentration-dependent accumulation of RGD-PEG$_{600}$-NPs-EPI and GGD-PEG$_{600}$-NPs-EPI on different cell lines (Fig. 7D). To examine whether RGD-motif is universal to improve various tumor cell binding and internalization, HeLa, HepG2 and SMMC7721 cell lines were adopted. Relatively low integrin expression has been shown in HeLa cells. HepG2 and SMMC7721 cells are metabolism cells. The results from different tumor cells were consistent with those from A375 cells, showing greater binding and internalization for RGD-PEG$_{600}$-NPs-EPI than GGD-PEG$_{600}$-NPs-EPI. Moreover, the internalization of RGD-PEG$_{600}$-NPs-EPI by liver metabolism cells (HepG2/SMMC7721) was approximate 3-fold higher than by epithelial cells (A375/HeLa), however, the binding in A375 cells (rich in integrins) can reach the same level (90–120%) as in liver metabolism cells (Fig. 7 C *vs.* D). These results suggested that the NPs uptake improved by RGD-PEG$_{600}$ depended on the type of cells.

In Vivo PD Study

The anti-tumor activities of EPI NPs were evaluated by tumor weight change in Kunming mice inoculated with S_{180} sarcoma. Tumor weight change reflects the pharmacodynamic action of different formulations. As shown in Fig. 8, the negative control groups showed the normal growth speed of tumors (groups 1 and 2; $p>0.05$, TGI≈0), but significantly decreased tumor weights were observed in RGD-PEG$_{600}$-NPs (group 3, TGI=25%). These results suggested an inherently weak antitumor effect of RGD-PEG$_{600}$.

NPs-EPI (group 5, TGI=44%) showed lower tumor weight than EPI solution (group 4, TGI=34%; $p<0.01$), suggesting NPs effectively deliver more EPI to tumors. RGD-NPs-EPI (group 13, TGI=53%) and NPs-EPI (group 5) showed no significant difference on tumor weight ($p>0.05$). GGD-PEG$_{600}$-NPs-EPI (group 6, TGI=47%) showed lighter tumor weight ($p<0.05$) than NPs-EPI (group 5), demonstrating the optimum stealth effect of pegylation. RGD-PEG$_{600}$-NPs-EPI (group 8, TGI=76%) showed much lighter tumor weight than GGD-PEG$_{600}$-NPs-EPI (group 6), RGD-NPs-EPI (group 13) and NPs-EPI (group 5). These results indicated RGD was the necessary sequence to ensure an affinity for integrins, while GGD had a minimal effect on the affinity. The conjugate of RGD-PEG$_{600}$ as an effective tumor targeting anchor modifying NPs was superior to pegylation or RGD alone for improved tumor selectivity.

RGD-PEG$_{4000}$-NPs-EPI (group 10, TGI=18%) showed high tumor weight as negative controls (groups 1 and 2; $p>0.05$), suggesting RGD-PEG$_{4000}$ failed in tumor targeting. However, RGD-PEG$_{300,\ 600\ \text{or}\ 1000}$-NPs-EPI (groups 7, 8 and 9) showed effectively low tumor weight, demonstrating favorable tumor targeting. There are significant differences in tumor weight between RGD-PEG$_{300}$-NPs-EPI and RGD-PEG$_{600}$-NPs-EPI (groups 7 and 8; $p<0.05$) and no differences between RGD-PEG$_{600}$-NPs-EPI and RGD-PEG$_{1000}$-NPs-EPI (groups 8 and 9; $p>0.05$). It may be explained that RGD-PEG $_{(Mw<300)}$ was easily fallen down from the NPs when the PEG chain was short, while RGD-PEG$_{4000}$ was tightly bound to NPs and thus prevented EPI release when the PEG chain was long. Both conditions will lead to the failure of EPI delivery to tumors. It is worth noting that longer PEG chain

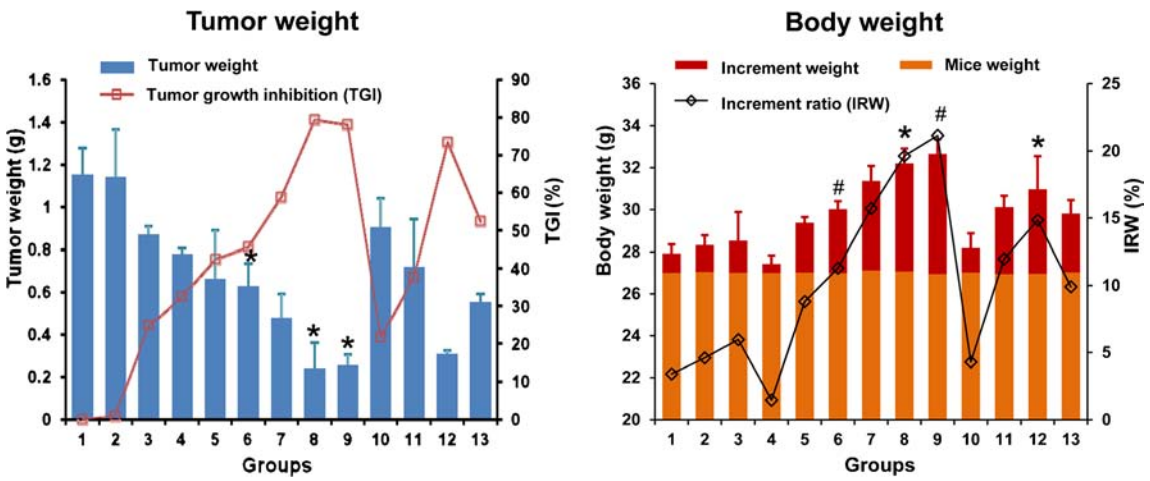

Fig. 8 Tumor weight and body weight changes (X ± SD, $n=10$) in mice bearing S_{180} sarcoma tumors after administration of different formulations in groups 1–13. (1) Saline; (2) NPs-PLLA; (3) RGD-PEG$_{600}$-NPs; (4) EPI solution; (5) NPs-EPI; (6) GGD-PEG$_{600}$-NPs-EPI; (7) RGD-PEG$_{300}$-NPs-EPI; (8) RGD-PEG$_{600}$-NPs-EPI; (9) RGD-PEG$_{1000}$-NPs-EPI; (10) RGD-PEG$_{4000}$-NPs-EPI; (11) RGD-PEG$_{600}$-NPs-EPI (1 mg/kg); (12) RGD-PEG$_{600}$-NPs-EPI (3 mg/kg); (13) RGD-NPs-EPI. The given dose of EPI in each group was 2 mg/kg or equivalent blank NPs amount unless pointed out specially. $^{*}p<0.05$, $^{\#}p<0.01$: group 6 (*vs.* group 5), group 8 and group 9 (*vs.* group 7), group 12 (*vs.* group 8).

(M_w = 4000) resulted in NPs aggregation in the experiments. The results demonstrated the appropriate molecular weights of PEG in RGD-PEG$_{Mw}$-NPs-EPI are 600 ~ 1000 in tested formulations to achieve improved tumor selectivity and decreased systemic exposure.

To further examine tumor targeting capacity of RGD-PEG$_{600}$, three doses of EPI (1, 2 and 3 mg/kg; group 11, 8, 12) in RGD-PEG$_{600}$-NPs-EPI were administered to tumor-bearing mice. There was no significant difference on tumor weight between groups given with 2 and 3 mg/kg dose. The anti-tumor activity of group 11 (1 mg/kg) was nearly half of that of group 8 (2 mg/kg). It suggested that the numbers of integrin receptors on tumor cell surface were limited and cellular uptake was near saturated for 2 mg/kg dose.

Body weight change was selected as an additional evaluation for anti-tumor activity of various EPI formulations since body weight loss is one form of cancer cachexia expression. Interestingly, the tendency of IRW from group 1 to group 13 in Fig. 8 is similar to that of TGI. However, EPI solution (group 4, IRW = 1.5%) showed the lowest body weight in all tested formulations, reflecting the intrinsic systemic side-effect of EPI. Various NPs effectively decreased systemic exposure of EPI and inhibited body weight loss. GGD-PEG$_{600}$-NPs-EPI (group 6, IRW = 11%) showed heavier body weight than NPs-EPI (group 5, IRW = 8.8%; $p < 0.01$), while RGD-NPs-EPI (group 13, IRW = 9.9%) showed no difference with NPs-EPI (group 5; $p > 0.05$). These results are consistent with those of tumor weight change. Interestingly, the body weight of group 12 (3 mg/kg, IRW = 15%) was a little lower than that of group 8 (2 mg/kg, IRW = 20%; $p < 0.05$). The possible reason is that 3 mg/kg dose did not raise the EPI amount in tumor site. Thus, higher concentration of EPI in blood circulation or normal tissues might increase risk for systemic exposure.

In Vivo PK Study

After the administration of three EPI-loaded formulations, i.e., EPI solution, NPs-EPI and RGD-PEG$_{600}$-NPs-EPI, the concentrations of EPI at different time points in the plasma, liver, heart, brain and tumor are displayed in Fig. 9 by using both the experiment data and the best-fit curves. Tables III and IV show the correspondingly fitting parameters of best-fit c-t equations. The best-fit c-t equations for three tested formulations in the tumor were formula zero, which suggested that EPI formulations slowly entered tumors with a duration parameter T of zero-order absorption. The T value of RGD-PEG$_{600}$-NPs-EPI was 6.4 and 6.8 times higher than NPs-EPI and EPI solution, respectively. RGD-PEG$_{600}$-NPs-EPI resulted in the maximum concentration in the plasma and tumor, minimum concentration in the liver, heart and brain, which was consistent with the calculation of AUC and CL. The AUC values of RGD-PEG$_{600}$-NPs-EPI were 1.4 and 2 times higher than NPs-EPI, and 1.8 and 3.6 times higher than EPI solution in the plasma and tumor, respectively. The reduced plasma clearance of RGD-PEG$_{600}$-NPs-EPI was mainly due to the increased system circulation after pegylation.

Statistical analysis further showed at the first time point (5 min), RGD-PEG$_{600}$-NPs-EPI had a similar plasma

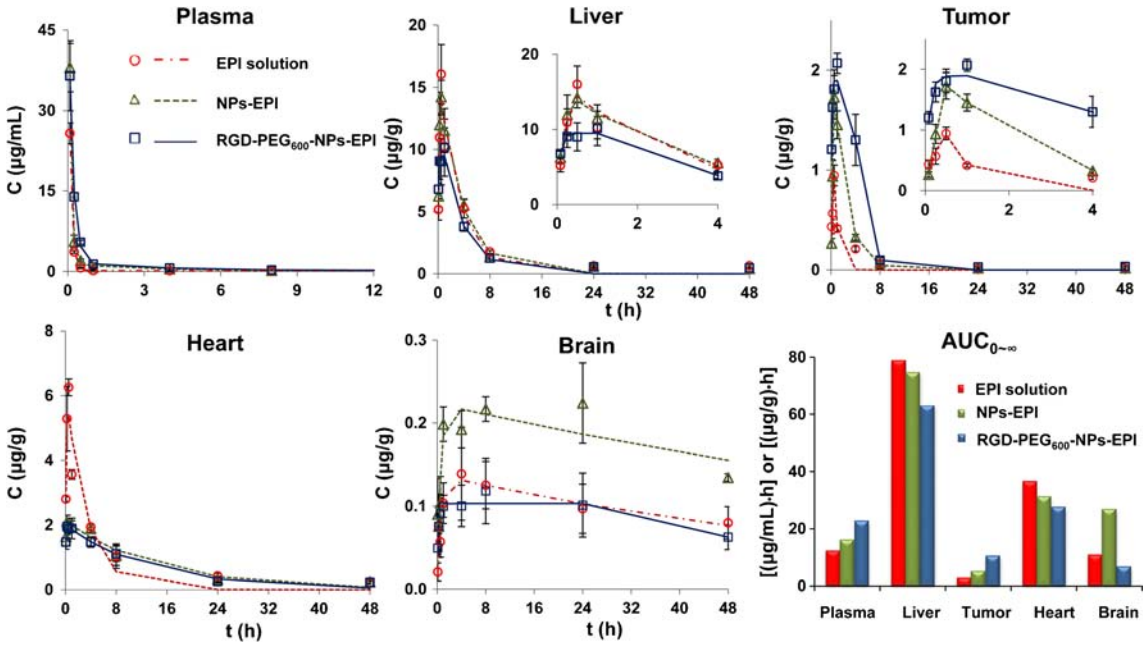

Fig. 9 EPI concentration (C) time (t) course studies in the plasma, liver, heart, brain and tumor of mice bearing S_{180} sarcoma tumors following tail vein injection of 8 mg/kg EPI solution, NPs-EPI and RGD-PEG$_{600}$-NPs-EPI, respectively. *Dots* represent experimental data. Mean ± SD, $n = 6$. *Corresponding lines* represent best-fit curves. The figure parts in liver and tumor from 0 to 4 h are magnified.

Table III Fitting Parameters of Best-Fit *c-t* Equations for EPI-Loaded Formulations in the Plasma

Preparation	Best-fit equation	Parameters				$AUC_{0\sim\infty}$ [(μg/mL)·h]	CL (mL/h)
		A (μg/mL)	α (h^{-1})	B (μg/mL)	β (h^{-1})		
EPI solution	Two-compart-ment model	66.444	11.519	0.156	0.023	12.478	12.823
NPs-EPI		104.067	12.571	1.407	0.274	16.232	9.857
RGD-PEG_{600}-NPs-EPI		54.588	5.566	1.495	0.200	22.953	6.971

concentration to NPs-EPI ($p>0.05$), but a higher tumor concentration than NPs-EPI ($p<0.01$). After the second time point (15 min), RGD-PEG_{600}-NPs-EPI showed a much higher plasma concentration than NPs-EPI ($p<0.01$). These results confirmed combination of RGD bioactive targeting effect and PEG stealth effect. Taking EPI solution as the *CDDS*, the RTI of RGD-PEG_{600}-NPs-EPI and NPs-EPI were 4.5 and 1.9, respectively. This result demonstrated that RGD-PEG_{600} enhanced tumor selectivity of NPs-EPI by ~2.4-fold.

Overall the NPs-EPI levels in plasma and most tissues fell between EPI solution and RGD-PEG_{600}-NPs-EPI levels. Among these three formulations, the concentrations of EPI solution were highest in the liver and heart but lowest in the plasma and tumor. On the other hand, the concentrations of RGD-PEG_{600}-NPs-EPI were highest in plasma and tumor but lowest in the liver and heart. Interestingly, NPs-EPI showed the maximum concentration in the brain, with 3.9 and 2.4 times higher AUC values than RGD-PEG_{600}-NPs-EPI and EPI solution, respectively. It implied that NPs-EPI might be a better formulation than RGD-PEG_{600}-NPs-EPI for brain tumor treatment. Differently, the best-fit c-t equations in the brain for both EPI solution and NPs-EPI were formula first with low elimination rate constant k_1 at around 0.01, while that for RGD-PEG_{600}-NPs-EPI was formula zero with a slow duration of zero-order absorption T at 29 h due to the stealth effect of pegylation and a little higher elimination rate constant k_2 at 0.03. The concentrations of various formulations in the brain were tiny owing to the blood–brain barrier (BBB).

DISCUSSION

Our study has developed novel PLLA nanoparticles modified by RGD-PEG conjugate to improve tumor-selectivity in cancer treatment. The desired objectives have been achieved by examining the structure of the conjugate, *in vitro* release, cellular kinetics, and *in vivo* PK and PD assessment. The promising results warrant our further studies to understand the role of slow degradation of PLLA in the EPI release from NPs and the associations between the chemical structure of the RGD-PEG conjugates, *in vitro* and *in vivo* characteristics.

The results of SEM, TEM, DSC and *in vitro* release analysis confirmed the binding of RGD-PEG on the surface of NPs spheres and the incorporation of EPI into the NPs in an high-energy amorphous form that makes EPI more soluble than the crystalline or hydrated form [14]. Thus, the release profile of EPI encapsulated in the NPs was improved. In addition, the

Table IV Fitting Parameters of Best-Fit *c-t* Equations for EPI-Loaded Formulations in Tissues

Tissues	Preparation	Best-fit equation	Parameters				$AUC_{0\sim\infty}$ [(μg/g)·h]
			A (μg/g)	k_1 (h^{-1})	k_2 (h^{-1})	T (h)	
Tumor	EPI solution	Formula zero	1.102	3.632	1.546	0.500	2.957
	NPs-EPI		9.523	0.402	0.489	0.530	5.268
	RGD-PEG_{600}-NPs-EPI		1.899	10.891	0.646	3.415	10.671
Liver	EPI solution	Formula zero	16.059	4.624	0.319	0.500	79.079
	NPs-EPI		14.818	6.610	0.283	0.451	74.780
	RGD-PEG_{600}-NPs-EPI		9.485	14.884	0.301	1.000	63.192
Heart	EPI solution	Formula first	6.349	0.305	8.537	–	36.830
	NPs-EPI		2.141	0.070	17.861	–	31.412
	RGD-PEG_{600}-NPs-EPI		2.001	0.076	16.311	–	27.827
Brain	EPI solution	Formula first	0.138	0.012	1.626	–	11.052
	NPs-EPI	Formula first	0.224	0.008	1.792	–	26.949
	RGD-PEG_{600}-NPs-EPI	Formula zero	0.103	6.032	0.026	28.816	6.904

characteristics of controlled and sustained drug release were observed. Firstly, the exothermic peak of crystallized RGD-PEG_{600} was found in the lyophilized NPs in the DSC thermogram, suggesting that RGD-PEG_{600} or PEG_{600} was partially exposed to the surface of NPs to some extent. The enhanced hydrophilic PEG chains on the surface could attract water molecules to form hydration membranes and subsequently decreased EPI release from NPs, and therefore influenced *in vitro* and *in vivo* trafficking of NPs [22, 26]. Secondly, the *in vitro* EPI release from RGD-PEG_{600}-NPs-EPI was faster in the medium with pH 5.4 than in pH 7.4, suggesting that NPs composed of PLLA and RGD-PEG_{600} were more likely to deliver abundant EPI to tumor site where the pH value is much lower than that in blood and normal tissues owing to excess lactic acid produced by hypoxia and acidic intracellular organelles [27]. This release profile implied tumor targeting effect with potential reduced systemic exposure and improved treatment outcomes. The expected results were shown in our *in vivo* PK and PD studies with 2-fold higher tumor AUC values of RGD-PEG_{600}-NPs-EPI than NPs-EPI accompanying with decreased distribution in liver, heart and brain.

Tumor HepG2 cell cycle and cytotoxicity tests further demonstrated the effective and sustained drug therapeutic effect of RGD-PEG_{600}-NPs-EPI until 72 h incubation. Firstly, RGD-PEG_{600}-NPs-EPI owned both active targeting (RGD binding to cell-surface integrin receptors) and hydration effect (pegylation), which adjusted cellular uptake at different time with higher membrane-bound and internalized EPI than GGD-PEG_{600}-NPs-EPI and NPs-EPI formulations. Secondly, the effect of RGD-integrin receptors binding on EPI NPs' intracellular transport was reflected by the ratio of internalization ($I_{(a)}/I_{(c)}$, a: RGD-PEG_{600}-NPs-EPI; c: GGD-PEG_{600}-NPs-EPI). Base on the concentration-dependent accumulation curves (Fig. 7C and D), the differences in average $I_{(a)}/I_{(c)}$ values between HeLa and A375/HepG2/SMMC7721 suggested that RGD-PEG_{600} might not effectively improve the amount of endocytosed NPs in cells with relatively low integrin expression [18]. Finally, Cellular uptake kinetics exhibited integrin receptor-dependent binding and internalization of RGD-PEG_{600}-NPs-EPI. The cellular uptake kinetic results were consistent with previous studies showing that internalization occurred mainly via endocytosis of the membrane-bound NPs and the proportional changes in I and B suggested first order rate process of internalization [28]. In addition, the improved binding and internalization were observed for all cell lines including low or high integrin expression tumor cells, suggesting the universal tumor cell selectivity of RGD-PEG_{600} motif.

The *in vivo* PD study did not find a significant difference in antitumor therapeutic effect between RGD-NPs-EPI and regular NPs-EPI. Tripeptide RGD alone might be easily cut from NPs, degraded by enzymes, and invalid for integrin-adhesion [24, 29]. However, once the linking group PEG_{Mw} (M_W=600~1000) was introduced to the formulations, the antitumor effect was enhanced. Firstly, the given RGD tripeptide might compete with the endogenous RGD sequence presenting in extracellular medium for binding integrins and inhibit integrin-mediated tumor cell adhesion and induce adhesion-dependent apoptosis [30]. Secondly, the molecular weight of PEG had an impact on the tumor targeting and therapeutic effects. Overall RGD-$PEG_{600–1000}$ demonstrated favorable antitumor effect. RGD-$PEG_{(Mw < 600)}$ were more likely to fall down from the NPs due to short PEG chain. On the other hand, RGD-$PEG_{(Mw > 1000)}$ tended to be bound to NPs tightly and prevented EPI release due to long PEG chain [23, 29]. Combined with the PK results, the optimal formulation with PEG_{Mw} (M_W=600~1000) was appropriate for further *in vivo* investigations to examine receptor-dependent tumor active-targeting effect.

CONCLUSION

A novel hydrophilic conjugate, RGD-PEG_{Mw} (M_W=300, 600, 1000), was synthesized and proved as an effective tumor active-targeting ligand in epirubicin loaded PLLA NPs. Tripeptide RGD is an integrin-adhesive ligand and easily broken off from NPs without the aid of PEG. PEG tightly connects RGD and NPs, and also avoids the uptake of MPS and BBB. *In vitro* release showed PLLA endowed a retard drug release and promoted drug release in acidic medium, benefiting *in vivo* trafficking to the acidic tumors. Cellular uptake kinetics showed RGD-PEG_{600} significantly improved tumor cell-surface binding and internalization of NPs by hepatic metabolism cells and integrin rich A375 cells. *In vivo* PD and PK studies further revealed the low systemic exposure and high anti-tumor therapeutic effect of RGD-PEG_{600}-NPs-EPI.

ACKNOWLEDGMENTS AND DISCLOSURES

This research was supported by the National Natural Science Foundation of China Grant 81202486 and Beijing Natural Science Foundation Grant 7133228.

REFERENCES

1. Kim J, Nam HY, Kim TI, Kim PH, Ryu J, Yun CO, *et al.* Active targeting of RGD-conjugated bioreducible polymer for delivery of oncolytic adenovirus expressing shRNA against IL-8 mRNA. Biomaterials. 2011;32(22):5158–66.
2. Park HS, Kim C, Kang YK. Preferred conformations of RGDX tetrapeptides to inhibit the binding of fibrinogen to platelets. Biopolymers. 2002;63(5):298–313.

3. Wang F, Cui C, Ren Z, Wang L, Liu H, Cui G. Preparation and biological evaluation of tumor-specific Ara-C liposomal preparations containing RGDV motif. J Pharm Sci. 2012;101(12):4559–68.
4. Du H, Cui C, Wang L, Liu H, Cui G. Novel tetrapeptide, RGDF, mediated tumor specific liposomal doxorubicin (DOX) preparations. Mol Parm. 2011;8(4):1224–32.
5. Li Y, Zheng X, Sun Y, Ren Z, Li X, Cui G. RGD-fatty alcohol-modified docetaxel liposomes improve tumor selectivity in vivo. Int J Pharm. 2014;468(1–2):133–41.
6. Zhang Y, Kohler N, Zhang M. Surface modification of superparamagnetic magnetitenanoparticles and their intracellular uptake. Biomaterials. 2002;23(7):1553–61.
7. Miller JS, Shen CJ, Leqant WR, Baranski JD, Blakely BL, Chen CS. Bioactive hydrogels made from step-growth derived PEG-peptide macromers. Biomaterials. 2010;13:3736–43.
8. Fairbanks B, Scott T, Kloxin C, Anseth K, Bowman C. Thiol-Yne photopolymerizations: novel mechanism, kinetics, and step-growth formation of highly cross-linked networks. Macromolecules. 2009;42: 211–7.
9. Xu Q, Liu Y, Su S, Li W, Chen C, Wu Y. Anti-tumor activity of paclitaxel through dual-targeting carrier of cyclic RGD and transferrin conjugated hyperbranched copolymer nanoparticles. Biomaterials. 2012;33(5):1627–39.
10. Kim KL, Han DK, Park K, Song SH, Kim JY, Kim JM, *et al.* Enhanced dermal wound neovascularization by targeted delivery of endothelial progenitor cells using an RGD-g-PLLA scaffold. Biomaterials. 2009;30(22):3742–8.
11. Zhang Q, Mochalin VN, Neitzel L, Hazeli K, Niu J, Kontsos A, *et al.* Mechanical properties and biomineralization of multifunctional nanodiamond-PLLA composites for bone tissue engineering. Biomaterials. 2012;33(20):5067–75.
12. Zhang HZ, Gao FP, Liu LR, Li XM, Zhou ZM, Yang XD, *et al.* Pullulan acetate nanoparticles prepared by solvent diffusion method for epirubicin chemotherapy. Colloids Surf B: Biointerfaces. 2009;71(1):19–26.
13. Shao W, Paul A, Zhao B, Lee C, Rodes L, Prakash S. Carbon nanotube lipid drug approach for targeted delivery of a chemotherapy drug in a human breast cancer xenograft animal model. Biomaterials. 2013;34(38):10109–19.
14. Chang LC, Wu SC, Tsai JW, Yu TJ, Tsai TR. Optimization of epirubicin nanoparticles using experimental design for enhanced intravesical drug delivery. Int J Pharm. 2009;376(1–2):195–203.
15. Shiraqa E, Barichello JM, Ishida T, Kiwada H. A metronomic schedule of cyclophosphamide combined with PEGylated liposomal doxorubicin has a highly antitumor effect in an experimental pulmonary metastatic mouse model. Int J Pharm. 2008;353(1–2):65–73.
16. Dash S, Murthy PN, Nath L, Chowdhury P. Kinetic modeling on drug release from controlled drug delivery systems. Acta Pol Pharm. 2010;67(3):217–23.
17. Ogawara K, Rots MG, Kok RJ, Moorlag HE, Van Loenen AM, Meijer DK, *et al.* A novel strategy to modify adenovirus tropism and enhance transgene delivery to activated vascular endothelial cells in vitro and in vivo. Hum Gene Ther. 2004;15(5):433–43.
18. Borgne-Sanchez A, Dupont S, Lanqonné A, Baux L, Lecoeur H, Chauvier D, *et al.* Targeted Vpr-derived peptides reach mitochondria to induce apoptosis of alphaVbeta3-expressing endothelial cells. Cell Death Differ. 2006;14(3):422–35.
19. Yang HW, Hua MY, Liu HL, Tsai RY, Pang ST, Hsu PH, *et al.* An epirubicin-conjugated nanocarrier with MRI function to overcome lethal multidrug-resistant bladder cancer. Biomaterials. 2012;33(15): 3919–30.
20. Pan H, Han L, Chen W, Yao M, Lu W. Targeting to tumor necrotic regions with biotinylated antibody and streptavidin modified liposomes. J Control Release. 2008;125(3):228–35.
21. Li Y, Zhu J. Modulation of combined-release behaviors from a novel "table-in-capsule system". J Control Release. 2004;95:381–9.
22. Jiang X, Sha X, Xin H, Chen L, Gao X, Wang X, *et al.* Self-aggregated pegylated poly (trimethylene carbonate) nanoparticles decorated with c(RGDyK) peptide for targeted paclitaxel delivery to integrin-rich tumors. Biomaterials. 2011;32(35):9457–69.
23. Song W, Tang Z, Zhang D, Zhang Y, Yu H, Li M, *et al.* Anti-tumor efficacy of c(RGDfK)-decorated polypeptide-based micelles co-loaded with docetaxel and cisplatin. Biomaterials. 2014;35(9):3005–14.
24. Bellis SL. Advantages of RGD peptides for directing cell association with biomaterials. Biomaterials. 2011;32(18):4205–10.
25. Li Y, Wang J, Gao Y, Zhu J, Wientjes MG, Au JL. Relationships between liposome properties, cell membrane binding, intracellular processing, and intracellular bioavailability. AAPS J. 2011;13(4):585–97.
26. Mao S, Shuai X, Unger F, Wittmar M, Xie X, Kissel T. Synthesis, characterization and cytotoxicity of poly(ethylene glycol)-graft-trimethyl chitosan block copolymers. Biomaterials. 2005;26(32): 6343–56.
27. Ko J, Park K, Kim YS, Kim MS, Han JK, Kim K, *et al.* Tumoral acidic extracellular pH targeting of pH-responsive MPEG-poly(beta-amino ester) block copolymer micelles for cancer therapy. J Control Release. 2007;123(2):109–15.
28. Li Y, Wang J, Wientjes MG, Au JL. Delivery of nanomedicines to extracellular and intracellular compartments of a solid tumor. Adv Drug Deliv Rev. 2012;64(1):29–39.
29. Veronese FM. Peptide and protein PEGylation: a review of problems and solutions. Biomaterials. 2001;22(5):405–17.
30. Ro H. Integrins: bidirectional, allosteric signaling machines. Cell. 2002;110(6):673–87.